analytical chemistry

Article

Single-Domain Antibodies for the Detection of SARS-CoV-2 Nucleocapsid Protein

George P. Anderson, Jinny L. Liu, Thomas J. Esparza, Bruce T. Voelker, E. Randal Hofmann, and Ellen R. Goldman*

Read Online

| ACCESS | | Metrics & More | | Article Recommendations | | Supporting Information |

ABSTRACT: The goal of this work was to develop recombinantly expressed variable domains derived from camelid heavy-chain antibodies known as single-domain antibodies (sdAbs) directed against the SARS-CoV-2 nucleocapsid protein for incorporation into detection assays. To achieve this, a llama was immunized using a recombinant SARS-CoV-2 nucleocapsid protein and an immune phage-display library of variable domains was developed. The sdAbs selected from this library segregated into five distinct sequence families. Three of these families bind to unique epitopes with high affinity, low nM to sub-nM K_D, as determined by surface plasmon resonance. To further enhance the utility of these sdAbs for the detection of nucleocapsid protein, homobivalent and heterobivalent genetic fusion constructs of the three high-affinity sdAbs were prepared. The effectiveness of the sdAbs for the detection of nucleocapsid protein was evaluated using MagPlex fluid array assays, a multiplexed immunoassay on color-coded magnetic microspheres. Using the optimal bivalent pair, one immobilized on the microsphere and the other serving as the biotinylated recognition reagent, a detection limit as low as 50 pg/mL of recombinant nucleocapsid and of killed virus down to 1.28×10^3 pfu/mL was achieved. The sdAbs described here represent immune reagents that can be tailored to be optimized for a number of detection platforms and may one day aid in the detection of SARS-CoV-2 to assist in controlling the current pandemic.
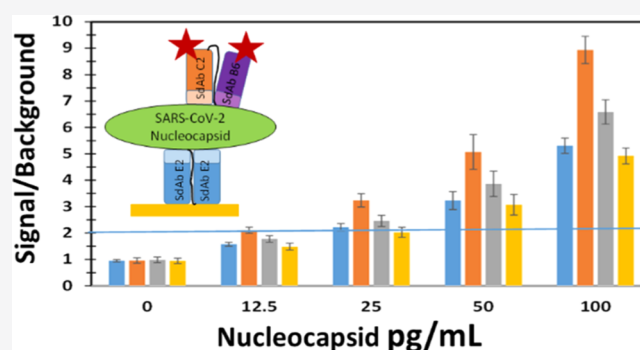
INTRODUCTION

Early diagnosis of infection with an emerging infectious respiratory virus, such as SARS-CoV-2, is particularly important not only to facilitate proper patient care but to ensure the safety of the community.[1] Detection methods have been rapidly improving due to the deepening understanding of COVID-19. Nucleic acid testing, chest computed tomography, confirmation of epidemiological history, and clinical manifestations are important bases for the diagnosis of COVID-19.[1−4] However, nucleic acid testing is time-consuming and very costly as it requires specific reagents, expensive specialized equipment, and skilled technicians. Additionally, nucleic acid tests can yield positive results after a patient is no longer in a period of high infectivity.[5] It is well accepted that a "positive" polymerase chain reaction (PCR) result reflects only the detection of viral RNA and does not necessarily indicate the presence of a viable virus. In comparison, the coronavirus antigen detection methods have the advantage of being rapid, less expensive, and relatively easy to perform. Thus, antigen-based testing provides a modality that complements the gold standard nucleic acid assays by filling in the testing gaps.

Viral antigen can serve as a specific marker for viral infection and significantly precedes the patient antibody response, often by days within infected people. In the case of SARS and SARS-CoV-2, the antigen can be detected up to 1 day before the appearance of clinical symptoms.[5,6] Additionally, antigen testing has the potential to identify those who have high levels of virus, making them likely to be highly infectious.[7] Thus, detection of the viral antigen fills the role for a rapid screening assay, achieving the critical early diagnosis required to limit further viral spread.

The SARS-CoV-2 genome is composed of approximately 30,000 nucleotides, which encodes four structural proteins: spike (S), envelope (E), membrane (M), and nucleocapsid (N) proteins.[8] These four main structural proteins are also found in other coronaviruses.[9] The N protein is highly immunogenic and abundantly expressed during infection.[10,11] After infection, the N protein enters the host cell together with the viral RNA to facilitate its replication and to process the
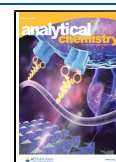
virus particle's assembly and release.[12] N has been detected in gargle solution samples and nasal swab samples of COVID-19 patients,[13−15] making it a promising target for antigen testing.

High-throughput MagPlex viral antigen assays have the advantage of being relatively fast and simple in comparison to PCR-based formats while providing the additional capability to be multiplexed.[16] MAGPIX, a simple and compact Luminex analyzer, makes the multiplexing method more affordable and robust without compromise with respect to the simplicity and high-throughput capacity.[17] Attractively, this same platform type can also be used as a read-out device for nucleic acid or antibody testing as well, allowing a single platform to fill multiple analytical purposes.[18,19] MagPlex fluid array assays on the MAGPIX instrument in conjunction with single-domain antibodies (sdAbs) provide an economical means to perform multiplexed assays, which can be expanded to include additional assays as desired or tested in a serial manner.

To date, commercial assays for SARS-CoV-2 N have relied upon conventional antibodies as the recognition reagents.[20,21] In the future, this role may be superseded by high-affinity sdAbs tailored to the detection platform enhancing the sensitivity and consistency of the detection methodology. Also known as nanobodies or VHHs, sdAbs are the antigen-binding fragments derived from the unconventional heavy-chain-only antibodies found in camelids, a family that includes camels, llamas, and alpacas.[22−24] They possess many advantages over conventional antibodies including remarkable stability, ability to bind to hidden epitopes, and can be engineered to work optimally for specific applications.[25] In addition, these antibodies are small and easily produced in good quantity in *Escherichia coli* or yeast. SdAbs have been tapped as potential therapeutics and prophylactics for SARS-CoV-2, with reports of several high-affinity sdAbs specific for S showing promise in preventing viral infection.[26,27] Multivalent sdAb constructs were demonstrated to further improve the neutralization potential.[28] In this report, we show that sdAbs directed toward N can be utilized for diagnostics; incorporating bivalent sdAb constructs into MagPlex assays led to improved detection over the standard sdAb constructs.

■ MATERIALS AND METHODS

Reagents. Chemical reagents were sourced from Sigma-Aldrich (St. Louis, MO, USA), Thermo Fisher Scientific (Waltham, MA, USA), or VWR International (Radnor, PA, USA) unless otherwise specified. Cloning enzymes, including restriction endonucleases and ligase, were obtained from New England Biolabs (Ipswich, MA, USA). DNA sequencing and gene synthesis were sourced through Eurofins Genomics (Louisville, KY, USA). Recombinant SARS-CoV-2 N (a) and recombinant SARS-CoV-2 receptor-binding domain (RBD) were acquired from ACROBiosystems (Newark, DE, USA). SARS-CoV-2 N (b), SARS-CoV NP, CoV-NP HKU1, CoV-NP OC43, MERS-CoV NP, CoV-NP-NL63, and CoV-NP 229E were obtained from East Coast Bio (North Berwick, ME, USA). Ebola virus-like particles (EBOV) from IBT Bioservices (Rockville, MD, USA) were obtained through the Joint Program Executive Office (JPEO) for Chemical, Biological, Radiological, and Nuclear Defense (CBRND) Joint Project Lead (JPL) CBRND Enabling Biotechnologies (EB) Defense Biological Product Assurance Office (DBPAO). Inactivated virus, gamma-irradiated SARS-CoV-2, was obtained from BEI Resources (Manassas, VA, USA).

Llama Immunizations. Llama immunizations were performed by Triple J farms (Bellingham, WA, USA). The immunization protocols used in this work were specifically approved by the Triple J Farms Institutional Animal Care and Use Committee (IACUC). One llama (Centavo) was immunized five times, each a week apart, with 100 μg of recombinant N. A week after the final boost, blood was drawn and used for the evaluation of Centavo's immune response as well as library construction. Peripheral blood mononuclear cells were isolated using Unisep tubes (Novamed), RNA was purified, and then cDNA was prepared. The variable heavy domains were amplified and cloned into the pecan 21 phage-display vector[29] to create an immune sdAb library.[30] Centavo's antibody titer was measured using the purified platelet-rich plasma.

Library Panning and Production of sdAb. A phage-display sdAb library derived from Centavo was used for the selection of sdAbs that recognize N. Two rounds of panning, using N adsorbed to wells of 96-well plates, were carried out essentially as previously described,[31] with the addition of a 20 min incubation in PBSM [phosphate-buffered saline (PBS) plus 4% powdered milk; weight/volume] between the sets of PBST (PBS plus 0.05% Tween 20) washes and PBS washes during round 2.

Monoclonal phage direct-binding MagPlex assays were employed to identify positive clones after the second round of panning.[32] Identified positive clones were re-streaked and subjected to DNA sequencing. We used the Multalin tool for the sequence alignment when comparing the protein sequences of positive clones.[33] A representative clone from each sequence family was mobilized from the pecan21 phage-display vector into the pET22b expression vector, through *NcoI* and *NotI* restriction sites, for protein production and characterization.[34] In addition, each sdAb was also cloned into a modified pET22b vector, which contained a hop tail, a c-terminal tail that was designed for the specific attachment of tags useful for multiple applications such as tracking, PEGylation for the improvement of serum half-life, or oriented immobilization.[35,36] Since the behavior of these sdAb versions was otherwise identical, for the purposes of this work, the variant utilized is not delineated other than in Table S1.

The pET22b-based sdAb expression plasmids were transformed into Tuner (DE3) for protein production. Freshly transformed colonies were used to start overnight cultures in 50 mL of terrific broth (TB) containing ampicillin (100 μg/mL) at 25 °C. The next day, the overnight cultures were poured into 450 mL of TB with ampicillin and grown for 2 h at 25 °C prior to induction with isopropyl-D-1 thiogalactoside (0.5 mM) and a further 2 h growth. Purification was carried out through an osmotic shock protocol, followed by immobilized metal affinity chromatography and fast protein liquid chromatography, as described previously.[37] The sdAb concentration was determined by UV absorption and stored at 4 °C or at −80 °C for long-term storage. All clones were found to produce well (Supporting Information, Table S1); NRL-N-B6 was the lowest at 2 mg/L, and other clones from this family may be tested in the future to examine if they produce better. As was seen previously, the hop tail did not affect protein production.[35] Although the hop tail is not necessary for MagPlex assays, it could facilitate the incorporation of these sdAbs into rapid formats in the future.

Production of Genetically Linked sdAbs. Genetically linked sdAbs were prepared using the strategy described

previously in which the first sdAb is flanked by *NcoI–NotI* restriction sites and the second sdAb is flanked by *BamHI–XhoI* restriction sites with a "GGGGSGGGGGSGGGGS" linker between them.[38] In this way, the sdAbs could be mixed-and-matched through swapping out the first or second sdAb component. Homobivalent and heterobivalent sdAb constructs were produced and purified using the same method as used for the standard sdAbs and is described above.

Circular Dichroism. Circular dichroism (CD) was performed in a Jasco J-815 spectropolarimeter using a quartz cuvette with a 1 cm pathlength. Each sdAb was diluted to 15 μg/mL in distilled water to a final volume of 3 mL. CD was measured at a wavelength of 205 nm as the stirred sample was heated from 25 to 85 °C at a rate of 2.5 °C/min (measured using an internal temperature probe), followed by cooling at the same rate to determine the percent refolding after heat denaturation. The change in total ellipticity between the starting 25 °C temperature and ending 85 °C was calculated, and the temperature at the midpoint based on this calculation was considered to be the melting temperature; error on these values was ±1 °C. The percentage ellipticity that recovered upon cooling was considered to be the refolding percentage; when evaluating refolding percentages, differences of 10% or less are not considered significant.

Surface Plasmon Resonance. Surface plasmon resonance (SPR) affinity and kinetic measurements were performed using the ProteOn XPR36 (Bio-Rad, Hercules, CA). Lanes of a general layer compact chip were individually coated with N covalently linked to the chip following the standard 1-ethyl-3-(3-dimethylaminopropyl) carbodiimide hydrochloride/N-hydroxysulfosuccinimide (sulfo-NHS) coupling chemistry available from the manufacturer. For these experiments, three lanes of the chip were coated with N in decreasing concentrations to ensure that the off rate was not being suppressed by rebinding after dissociation due to the ligand being present at too high a concentration on the surface. After the ligand was immobilized, the chip was rotated 90° to allow the binding of the sdAb to be tested at a range of concentrations simultaneously. The chip was then regenerated, and the next sdAb was evaluated. Binding kinetics of each antibody was tested at 25 °C by flowing six concentrations of each sdAb varying from 300 to 0 nM at 100 μL/min for 90 s over the antigen-coated chip and then monitoring dissociation for 600 s. The data were analyzed using a global Langmuir fit, and the standard error was always less than 10%, typically ~1%; variation between multiple tests of the same sample was less than a factor of 2, and a representative data set is used in Table 1 and is shown in the Supporting Information, Figure S3. The results obtained were well within the working range of the instrument, with an association constant (k_a) of 3×10^3–3×10^6 M^{-1} s^{-1} and a dissociation constant of 1×10^{-6}–6×10^{-1} s^{-1}.

MagPlex Direct-Binding and Sandwich Assays. Specificity and an indication of affinity were appraised via the direct binding of the sdAb to SARS-CoV-2 N recombinant protein immobilized on MagPlex magnetic microspheres (Luminex, Austin, TX, USA). The SARS-CoV-2 N, along with RBD, was immobilized to unique sets of MagPlex microspheres using the standard immobilization protocol provided by the manufacturer. To prepare the biotinylated (Bt) tracer reagent, 10-fold excess of EZ-Link NHS-LC-LC-Biotin (Thermo Fisher Scientific) was added to 300 μg of each sdAb at 1 mg/mL for 30 min; excess biotin was removed using Zeba spin columns (Thermo Fisher Scientific). The

**Table 1. SPR Affinity Determinations of Both Standard and Bivalent sdAbs**[a]

clone	k_a (1/M s)	k_d (1/S)	K_D (nM)
NRL-N-A9	NSB	NSB	NSB
NRL-N-E10	6.9×10^4	9.5×10^{-4}	14
NRL-N-E2	3.5×10^5	2.7×10^{-4}	0.8
NRL-N-C2	1.6×10^5	1.8×10^{-4}	1.1
NRL-N-B6	1.9×10^5	3.0×10^{-4}	1.6
C2–C2	2.7×10^5	3.9×10^{-5}	1.4
E2–E2	6.6×10^6	3.4×10^{-4}	0.05
E2–B6	1.4×10^6	3.7×10^{-4}	0.3
E2–C2	2.4×10^6	2.9×10^{-4}	0.1
C2–B6	2.7×10^5	1.6×10^{-4}	0.6

[a]NSB—non-specific binding.

absorbance at 280 nM was used to calculate the concentration of Bt-sdAb. Dilutions of each Bt-sdAb in PBSTB [PBS + 0.05% Tween + 0.1% bovine serum albumin (BSA)] were prepared in round-bottom polypropylene microtiter plates (VWR). The mixture of antigen-coated MagPlex microspheres was added to the wells. The plate was washed using PBST while placed on a 96f magnet (BioTek, Winooski, VT), incubated with 5 μg/mL streptavidin-R-phycoerythrin ([SA–PE] Molecular Probes, Eugene, OR) for 30 min, and then washed, and then binding was evaluated on the MAGPIX instrument (Luminex, Austin, TX).

Sandwich format MagPlex bead assays were performed in order to demonstrate the ability of the sdAbs to act as both the capture and recognition reagent for the detection of N. For these assays, each sdAb was immobilized to a set of MagPlex microspheres as described above and then tested for its ability to function as a capture antibody. Initial tests evaluated all the clones as both the immobilized capture and the Bt recognition molecule in the assay. To improve the limit of detection (LOD) for N, the same assay format was repeated using the hetero- and homobivalent constructs of the three best sdAbs. For the amplified LOD assay using the standard sdAb reagents, the N was diluted into PBST with 1 mg/mL BSA, as were all the other assay reagents, and then further diluted on a round-bottom polypropylene microtiter plate. Then, the sdAb-coated microspheres were added to provide a minimum of 50 microspheres for each set per well and incubated for 30 min. In most tests, assay process-control microspheres were included but not shown to simplify the graphs.[39] The plate was washed with PBST and incubated with the desired Bt-sdAb at 1 μg/mL for 30 min. To generate the fluorescent signal, the plate was washed and then incubated sequentially with 50 μL of SA–PE at 5 μg/mL in each well for 15 min, washed again, then incubated with 50 μL of Bt goat anti-streptavidin (Bt-goat-anti-SA) from Vector Laboratories (Burlingame, CA) at 1 μg/mL for 15 min, washed, and finally incubated with SA–PE as before. Then, the plate was washed a final time prior to being evaluated on the MAGPIX. A ratio of 2 for the signal/background was utilized as the LOD as this ratio provides a signal that assures a difference that is greater than 3 times the standard deviation (SD) of the mean of both the background and the data point considered significant. The assay for the LOD for N using the bivalent sdAb reagents was similar to the above protocol other than the fact that the incubation step with N was extended to 1 h and that the N and all subsequent reagents were diluted into a 1:1 mixture of PBST and
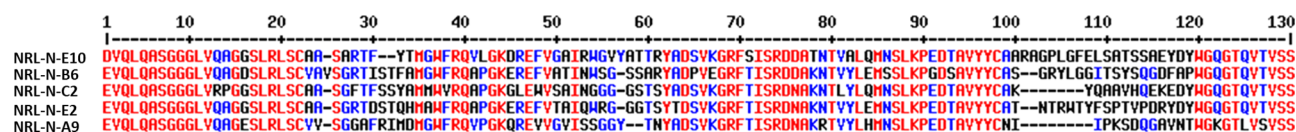
Figure 1. Sequence alignment of sdAbs that bind recombinant SARS-CoV-2 N. Sequences are given in the single-letter amino acid code. Alignment was performed using Multalin.[33] Red denotes high homology position, while blue indicates lower homology. Numbering is sequential based on the NRL-N-E10 sequence. Using this numbering scheme, we define CDR1 as the region of amino acid residues 26−35, CDR2: 50−65, and CDR3: 99−119.

LowCross Buffer (Candor, Wangen, Germany), which had been previously observed to improve assay sensitivity.[39]

■ RESULTS AND DISCUSSION

In order to generate sdAbs toward the N of SARS-CoV-2, a llama was first immunized with recombinant N. Once a successful immune response toward N was confirmed (Supporting Information, Figure S1), a phage-display library was prepared to capture the immune repertoire of heavy-chain antibody variable domains. After two rounds of panning on SARS-CoV-2 N, we examined 96 distinct phages using a direct-binding MagPlex assay, where N was covalently attached to the microsphere and the amount of phage bound to the surface was indicated by the addition of an anti-M13-mAb−phycoerythrin conjugate. Sixteen positive clones with a signal on N at least 5 times the signal on the RBD portion of the spike protein were chosen for sequencing, which revealed five unique sequence families (Supporting Information, Figure S2). Sequence families are defined as a group of sdAbs sharing near identical complementarity-determining regions (CDRs). The sequences of representative clones from each of the families selected for production and further testing are shown in Figure 1. Eight clones made up the NRL-N-B6 sequence family; five were in the NRL-N-E2 family, whereas NRL-N-C2, NRL-N-E10, and NRL-N-A9 were each single-member families. For brevity, the clones are often referred to by a shortened notation consisting of only the letter and number designation.

Soluble protein was produced for each of these five clones; most produced well with yields between 2 and 37 mg/L (Supporting Information, Table S1). They were then examined by a direct-binding MagPlex assay to confirm specificity to N (Figure 2), while the affinity for each clone was determined by SPR (Table 1 and Supporting Information, Figure S3). Both the direct-binding MagPlex and SPR showed that clones E2, B6, and C2 outperformed both E10 and A9. In fact, clone A9 showed no specific binding as assessed by SPR and was not considered further. This was indicative that although the presence of negative control microspheres coated with RBD allowed the elimination of some of the clones that exhibited nonspecific binding in the initial phage-display screening, it was not a foolproof process. The thermal stability and ability to refold for the four specific sdAbs were evaluated by CD (Supporting Information, Table S1). The sdAbs displayed melting temperatures ranging from 55 to 70 °C and refolding of between 41 and 87% after heat denaturation; however, both of those properties can be improved through protein engineering.[40] Differences in refolding percentages are only significant in broad ranges, where good refolding is 85% or better, moderate refolding being 50−85%, and poor refolding less than 50%. These values can easily be improved by lowering the isoelectric point of the sdAb, which has been seen to yield refolding percentages near 100%.[35,41]
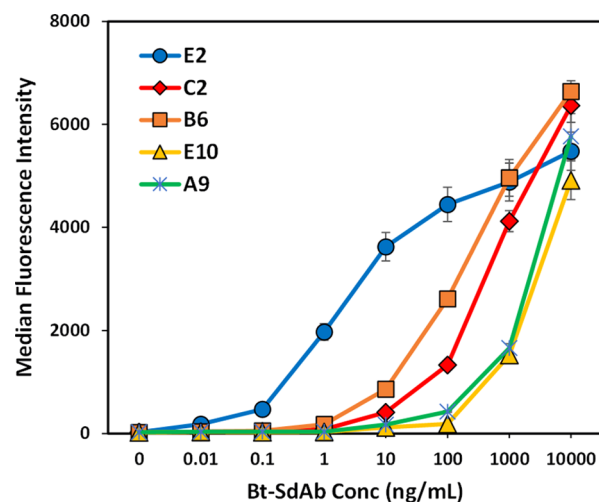

Figure 2. Direct-binding MagPlex assay to determine the ability of purified representatives from each of the five sequence families binding to the bead-immobilized N. Two sets of N-coated microspheres were averaged with the error bars (standard error of the mean) shown, along with a set of RBD-coated microspheres which had little-to-no signal and are not shown.

Affinity is just one measure of utility; binders with sub-nM K_D all have sufficient affinity to have utility in detection assays and require empiric testing to determine the best binder or binding pair for the application being optimized. While direct-binding assays are good for demonstrating the binding ability and assessing specificity, antibody reagents ultimately need to work in a sandwich format for most antibody-based diagnostic assays. Because clones E2, B6, and C2 appeared to have the best binding characteristics of the five, we focused on integrating them into a sandwich format. First, by immobilizing each sdAb onto microspheres, we performed a checkerboard assay that indicated that each sdAb binds to a distinct epitope on N (Figure 3). Although native N is multimeric in nature,[42] our data suggest that the recombinant N is monomeric as it can be seen that none of the sdAbs works efficiently as both capture and tracer; however, each can be paired with either of the other two.

A dose−response curve to assess detection limits with the different sdAb pairs revealed that E2 was the best capture, providing detection down to about 1 ng/mL when paired with either B6 or C2 as tracers (Figure 4). Although this is a good starting point, a lower level of detection is required for a useful diagnostic assay.

Multivalent sdAbs have proven superior to standard sdAbs for the neutralization of several viruses including SARS-CoV-2.[28,43] Multivalent sdAbs can provide increased apparent affinity through avidity,[38,44] making them advantageous for use in detection assays; we have seen improved detection of several targets incorporating multivalent capture reagents.[39] As the E2
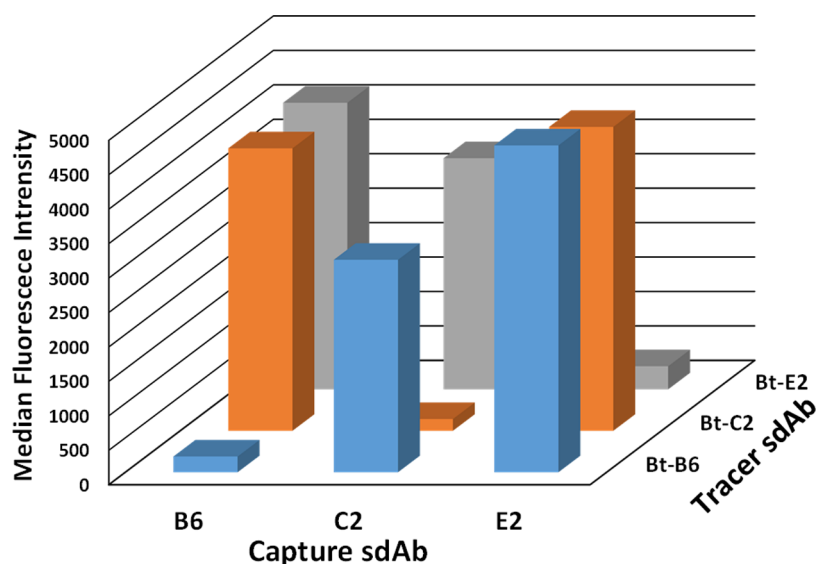
Figure 3. Checkerboard format sandwich MagPlex assay in which each of the three sdAbs is paired with itself and the other two. None of the sdAb captures works well with itself as a Bt tracer, but each functions with the other two.
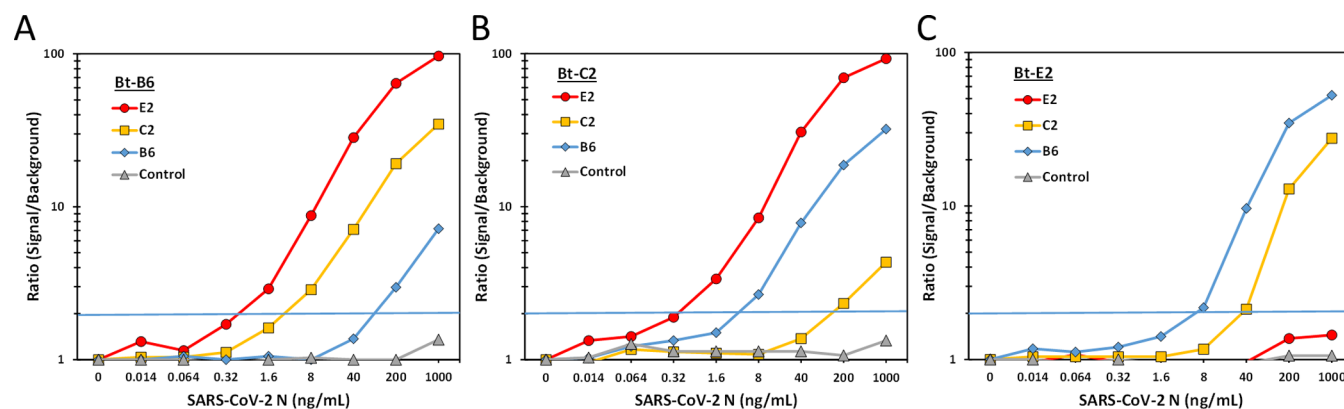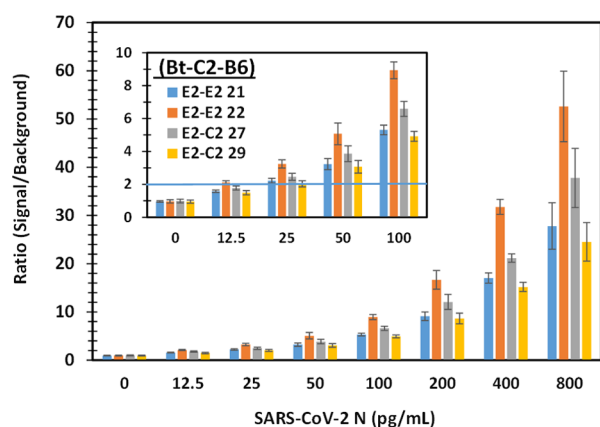

Figure 4. MagPlex amplified sandwich fluid array assay for the detection of SARS-CoV-2 N using each sdAb as the Bt tracer with each sdAb on a separate capture microsphere set. The control shown was a MagPlex set coated with sdAb toward an unrelated target. The assay was done in an amplified format, as described in the Materials and Methods, with a ratio of 2 (signals divided by background) being considered the LOD. Bt-tracer—A: Bt-B6, B: Bt-C2, and C: Bt-E2.

was the best capture and recognizes a different epitope than C2 and B6, we chose to construct a bivalent version of E2 as well as combine E2 with C2 and B6 and combine C2 with B6. We also made a C2−C2 construct to determine if the bivalent version would prove to be a better capture reagent. Direct-binding MagPlex assays showed that the E2−B6 and E2−C2 heterobivalent constructs were much better than the standard sdAbs, while the other constructs did not perform much different in this format (Supporting Information, Figure S4). Analysis by SPR (Table 1) showed that with the exception of C2−C2, the other bivalent constructs all had sub-nM affinity for N, thus achieving the avidity, an apparent enhanced affinity, which was desired.

The bivalent sdAbs were incorporated into sandwich assays as both capture and tracer reagents. The E2−E2 and E2−C2 captures in conjunction with the Bt-C2−B6 tracer yielded the best results; dose−response curves were evaluated in preliminary experiments for all the reagents (not shown). To achieve consistent high sensitivity, it was necessary to utilize a two-step amplification where the initial signal generated by SA−PE is amplified by the addition of a layer of Bt-goat anti-

SA, followed by a second layer of SA−PE. This amplification method has been found to provide little advantage for conventional antibodies but has shown to improve MagPlex assays using sdAbs by a factor of 5 or better.[32,45] Using this protocol, we obtained a LOD for N of 50 pg/mL (Figure 5). This same assay was evaluated for the detection of the killed virus where all the viral components are present; a LOD of 1.28×10^3 pfu/mL killed virus was obtained using E2−C2 as the capture reagent (Figure 6). These LODs suggest that this method may be successful for the detection of SARS-CoV-2 in actual patient samples, the next step in the transition to obtaining an Emergency Use Authorization.

This MagPlex assay has the advantage of showing good sensitivity while being low cost and having a high throughput. One can prepare 96 samples in about 2 h and they can be evaluated on the MAGPIX instrument in less than 1 h. One challenge of using the amplification step is maintaining a low background. Initial studies showed a signal response at equally low concentrations, but it did not always achieve the desired LOD or a consistent dose response. By using 1:1 PBST/LowCross buffer for the sample and all assay reagents,

Figure 5. MagPlex sandwich fluid array assay for the detection of SARS-CoV-2 N (a) using two sets of E2−E2 and E2−C2 as the capture on the MagPlex bead indicated in the legend and Bt-C2−B6 as the tracer in an amplified assay, as described in the Materials and Methods. A dose−response bar graph for an experiment conducted with eight replicates at each concentration is shown; error bars represent the SD of those eight replicates. This experiment was repeated three times, once as shown, once in quadruplicate, and once in triplicate, all giving similar results. A ratio of 2 (signal divided by a background) is considered the LOD.
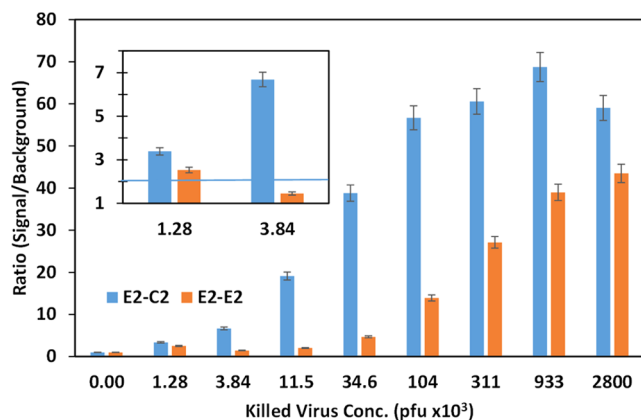
Figure 6. MagPlex amplified sandwich immunoassay for the detection of killed SARS-CoV-2 virus using the E2−C2 and E2−E2 captures paired with the Bt-C2−B6 tracer. The inset shows the two lowest concentrations to allow visualization of the LOD. The error bars shown represent the average % CV of the data.

consistent sensitive results were obtained.[39] The challenge will be to achieve these results with actual samples.

At this point, we also desired to investigate the cross reactivity of these reagents. MagPlex microspheres coated with E2, C2, B6, E2−E2, and E2−C2 were combined and tested simultaneously with each as the Bt tracer antibody. Since E2−C2 was functional as a capture for each of the Bt sdAb used as the tracer antibody, only that set is shown in Figure 7. Figure 8 shows the results with the E2−E2 capture and the Bt-C2−B6 tracer; additional data are not shown as the data presented provided the illuminating findings. The tracers that included B6 have strong cross reactivity to SARS-CoV N; otherwise, these reagents show good selectivity with cross reactivity to the other NP variants observed only at high concentrations. It is not surprising to observe cross reactivity with the SARS-CoV N as high similarity (over 87%) has been noted between the N

sequence of SARS-CoV-2 and the N sequence of other β coronaviruses (i.e., SARS-CoV).[46] As both of these coronaviruses can be associated with severe diseases, this cross reactivity should not be a liability for an assay built with the sdAbs, especially as MagPlex assays can easily be multiplexed. It appears that E2 has much better selectivity than the other sdAbs, so it would be possible to detect and discriminate both SARS-CoV and SARS-CoV-2 simultaneously using multiple capture bead sets. This is confirmed in Figure 8, where the response to SARS-CoV NP was much less for E2−E2 as the capture molecule than that was observed for E2−C2 in Figure 7.

Although we have not performed the more extensive inclusivity and exclusivity panels that would be necessary prior to moving this assay to actual patient sample testing, our limited panels in combination with the fact that these sdAb constructs do not bind either RBD or the EBOV indicate that they have good specificity. Another potential concern is the ability of diagnostic reagents to recognize N variants. Although one would not expect the binding to N to be under the same evolutionary pressure to develop an escape mutant that binding to the RBD of the S protein is under, substitutions are found within the N. An examination of N from over 38,000 SARS-CoV-2 sequences showed that mutations cluster in the linker region between the RNA-binding domain and the dimerization domain.[47] Future studies to elucidate the epitopes of the N-binding sdAbs would be helpful in determining if they bind in the conserved regions of N or in regions more prone to substitutions.

■ CONCLUSIONS

There have been numerous reports of sdAbs developed toward SARS-CoV-2 S for the development of therapeutics, the first published among these detailed sdAbs originally selected for their binding to S from SARS-CoV.[48] In addition to sdAbs derived from camelids, SARS-CoV-2 S binders have also been derived from a semisynthetic library of human variable heavy domains.[49] Currently, there are almost no literature reports describing SARS-CoV-2 N binding sdAbs; one report details N binders selected from a semisynthetic llama library.[50] We have selected sdAbs from an immune llama library that are specific for three different epitopes on the N of SARS-CoV-2. These three sdAbs bind with high affinity, and by the formation of heterobivalent and homobivalent constructs, we were able to achieve sub-nM affinities. Selecting the best pairs of bivalent constructs, we developed a MagPlex fluid array assay that achieved a LOD of 50 pg/mL for N and 1.28×10^3 pfu/mL for the killed virus. Specificity testing showed significant binding to only the N of SARS-CoV-2 and SARS-CoV, indicating highly selective binding. In addition, it should also be possible to further improve the sensitivity of detection on the MAGPIX platform, as a neither a means to orient the capture molecule, nor peptide tail additions that allow for increased biotinylation were applied to these constructs.[39,51] Furthermore, it should be possible to engineer these same sdAbs to possess enhanced thermal stability or optimize them to enable the sensitive detection of SARS-CoV-2 on other detection platforms. Other applications focused toward the use of these sdAbs as therapeutics might also be envisioned. This work, by inclusion of the sequences of sdAbs discovered here, enables those efforts to proceed unfettered and hopefully can provide additional tools to help defeat this ongoing pandemic.
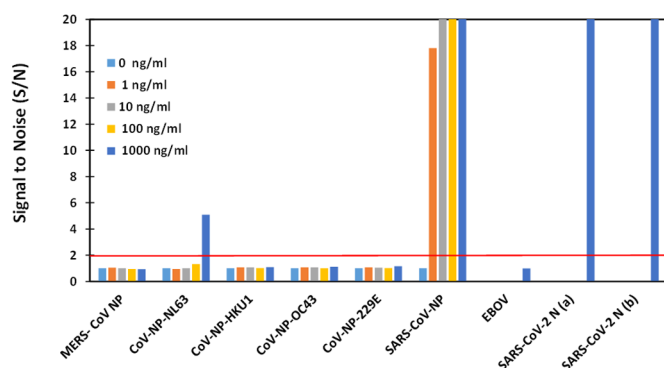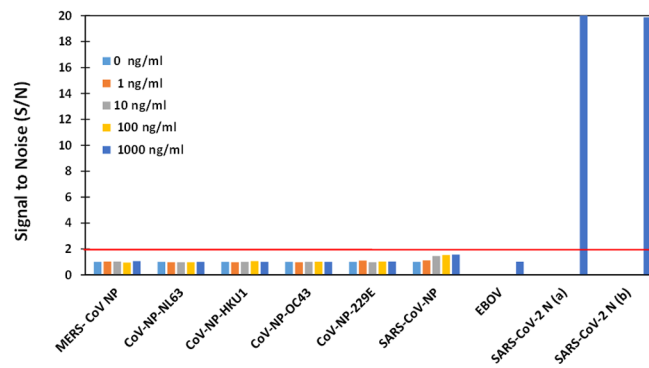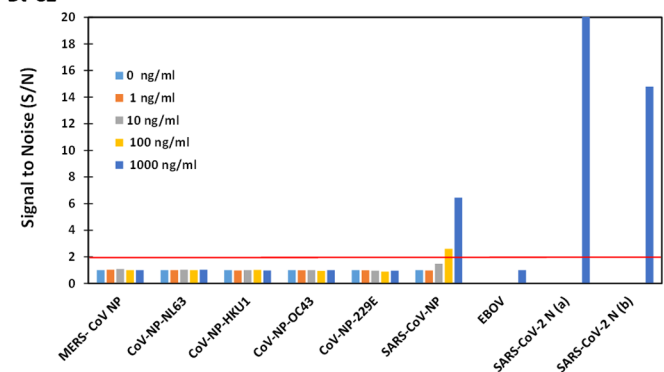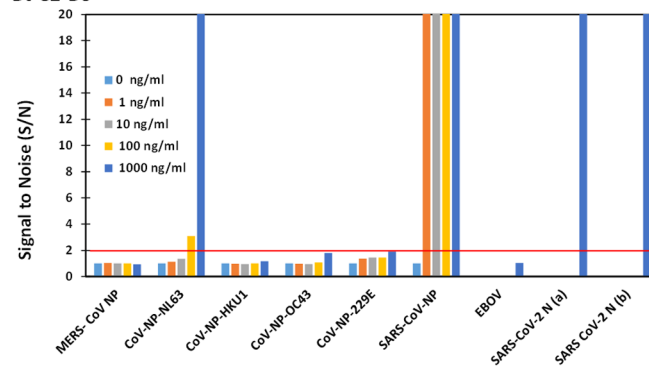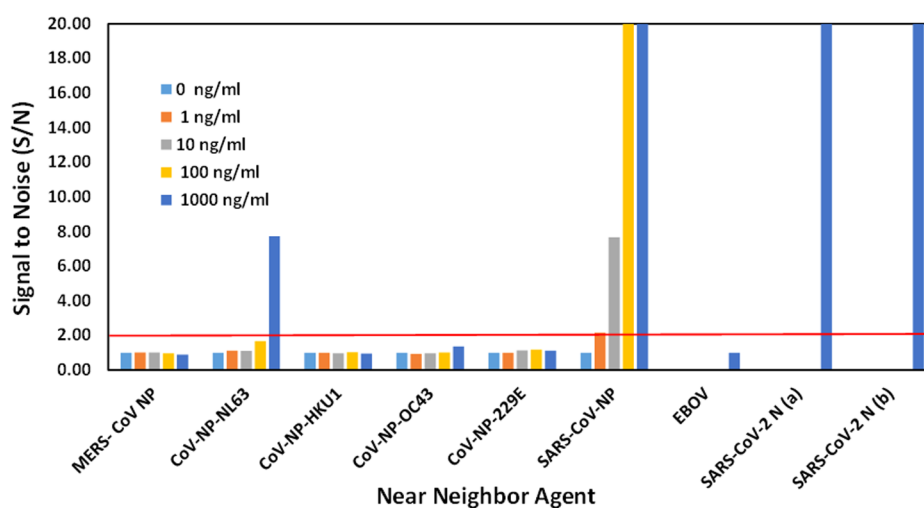
Figure 7. MagPlex sandwich fluid array assay for the cross reactivity of the sdAb reagents. Shown is the assay using the E2−C2 capture and B6, E2, C2, and C2−B6 as indicated as the Bt tracer reagent. NP-NL63 is a truncation including aa 221−340. The two positive controls are recombinant SARS-CoV-2 N from two different sources, as described in the Materials and Methods.

Figure 8. MagPlex sandwich fluid array assay for the cross reactivity testing using E2−E2 as the capture and Bt-C2−B6 as the tracer reagent. These results show much less binding of SARS-CoV NP than was observed in Figure 7 when E2−C2 acted as the capture with the Bt-C2−B6 tracer. NP-NL63 is a truncation including aa 221−340. The two positive controls are recombinant SARS-CoV-2 N from two different sources, as described in the Materials and Methods.

■ ASSOCIATED CONTENT

Ⓢ Supporting Information

The Supporting Information is available free of charge at https://pubs.acs.org/doi/10.1021/acs.analchem.1c00677.

> Evaluation of the llama serum, sequence alignment, SPR data, bivalent construct direct binding, sdAb production, melting point, and refolding potential (PDF)

■ AUTHOR INFORMATION

Corresponding Author

Ellen R. Goldman − *Center for Biomolecular Science and Engineering, US Naval Research Laboratory, Washington, District of Columbia 20375, United States;* ⓞ orcid.org/0000-0001-9533-7455; Phone: 202-404-6052; Email: ellen.goldman@nrl.navy.mil

Authors

George P. Anderson − *Center for Biomolecular Science and Engineering, US Naval Research Laboratory, Washington, District of Columbia 20375, United States*

Jinny L. Liu − *Center for Biomolecular Science and Engineering, US Naval Research Laboratory, Washington, District of Columbia 20375, United States*

Thomas J. Esparza − *Laboratory of Functional and Molecular Imaging, The National Institute of Neurological Disorders and Stroke Intramural Research Program, Bethesda, Maryland 20892, United States; Henry M. Jackson Foundation for the Advancement of Military Medicine, Bethesda, Maryland 20892, United States*

Bruce T. Voelker − *Chemical Biological Center, U.S. Army Combat Capabilities Development Command, Aberdeen Proving Ground, Maryland 21010, United States*

E. Randal Hofmann − *Chemical Biological Center, U.S. Army Combat Capabilities Development Command, Aberdeen Proving Ground, Maryland 21010, United States; EXCET, Inc., Springfield, Virginia 22150, United States*

Complete contact information is available at:
https://pubs.acs.org/10.1021/acs.analchem.1c00677

◼ REFERENCES

(1) Sabino-Silva, R.; Jardim, A. C. G.; Siqueira, W. L. *Clin. Oral Invest.* **2020**, *24*, 1619−1621.

(2) Wang, Y.; Kang, H.; Liu, X.; Tong, Z. *J. Med. Virol.* **2020**, *92*, 538−539.

(3) Zu, Z. Y.; Jiang, M. D.; Xu, P. P.; Chen, W.; Ni, Q. Q.; Lu, G. M.; Zhang, L. J. *Radiology* **2020**, *296*, E15−E25.

(4) Pan, F.; Ye, T.; Sun, P.; Gui, S.; Liang, B.; Li, L.; Zheng, D.; Wang, J.; Hesketh, R. L.; Yang, L.; Zheng, C. *Radiology* **2020**, *295*, 715−721.

(5) Sethuraman, N.; Jeremiah, S. S.; Ryo, A. *J. Am. Med. Assoc.* **2020**, *323*, 2249−2251.

(6) Che, X.-Y.; Hao, W.; Wang, Y.; Di, B.; Yin, K.; Xu, Y.-C.; Feng, C.-S.; Wan, Z.-Y.; Cheng, V. C. C.; Yuen, K.-Y. *Emerg. Infect. Dis.* **2004**, *10*, 1947−1949.

(7) Guglielmi, G. *Nature* **2020**, *585*, 496−498.

(8) Lu, R.; Zhao, X.; Li, J.; Niu, P.; Yang, B.; Wu, H.; Wang, W.; Song, H.; Huang, B.; Zhu, N.; Bi, Y.; Ma, X.; Zhan, F.; Wang, L.; Hu, T.; Zhou, H.; Hu, Z.; Zhou, W.; Zhao, L.; Chen, J.; Meng, Y.; Wang, J.; Lin, Y.; Yuan, J.; Xie, Z.; Ma, J.; Liu, W. J.; Wang, D.; Xu, W.; Holmes, E. C.; Gao, G. F.; Wu, G.; Chen, W.; Shi, W.; Tan, W. *Lancet* **2020**, *395*, 565−574.

(9) Fehr, A. R.; Perlman, S. Coronaviruses: An Overview of Their Replication and Pathogenesis. In *Coronaviruses: Methods and Protocols*; Maier, H. J., Bickerton, E., Britton, P., Eds.; Springer New York: New York, NY, 2015; pp 1−23.

(10) Shang, B.; Wang, X.-Y.; Yuan, J.-W.; Vabret, A.; Wu, X.-D.; Yang, R.-F.; Tian, L.; Ji, Y.-Y.; Deubel, V.; Sun, B. *Biochem. Biophys. Res. Commun.* **2005**, *336*, 110−117.

(11) Liu, S.; Leng, C.; Lien, S.; Chi, H.; Huang, C.; Lin, C.; Lian, W.; Chen, C.; Hsieh, S.; Chong, P. *Vaccine* **2006**, *24*, 3100−3108.

(12) Narayanan, K.; Chen, C.-J.; Maeda, J.; Makino, S. *J. Virol.* **2003**, *77*, 2922−2927.

(13) Nikolaev, E. N.; Indeykina, M. I.; Brzhozovskiy, A. G.; Bugrova, A. E.; Kononikhin, A. S.; Starodubtseva, N. L.; Petrotchenko, E. V.; Kovalev, G. I.; Borchers, C. H.; Sukhikh, G. T. *J. Proteome Res.* **2020**, *19*, 4393−4397.

(14) Young, S.; Taylor, S. N.; Cammarata, C. L.; Varnado, K. G.; Roger-Dalbert, C.; Montano, A.; Griego-Fullbright, C.; Burgard, C.; Fernandez, C.; Eckert, K.; Andrews, J. C.; Ren, H.; Allen, J.; Ackerman, R.; Cooper, C. K. *J. Clin. Microbiol.* **2020**, *59*, No. e02338-20.

(15) Gouveia, D.; Miotello, G.; Gallais, F.; Gaillard, J.-C.; Debroas, S.; Bellanger, L.; Lavigne, J.-P.; Sotto, A.; Grenga, L.; Pible, O.; Armengaud, J. *J. Proteome Res.* **2020**, *19*, 4407−4416.

(16) Kim, J. S.; Taitt, C. R.; Ligler, F. S.; Anderson, G. P. *Sens. & Instrumen. Food Qual. Saf.* **2010**, *4*, 73−81.

(17) Mechaly, A.; Vitner, E.; Levy, H.; Weiss, S.; Bar-David, E.; Gur, D.; Koren, M.; Cohen, H.; Cohen, O.; Mamroud, E.; Fisher, M. *J. Clin. Microbiol.* **2018**, *56*, No. e01479-17.

(18) Boyd, V.; Smith, I.; Crameri, G.; Burroughs, A. L.; Durr, P. A.; White, J.; Cowled, C.; Marsh, G. A.; Wang, L.-F. *J. Virol. Methods* **2015**, *223*, 5−12.

(19) Chen, J. H.-K.; Yip, C. C.-Y.; Chan, J. F.-W.; Poon, R. W.-S.; To, K. K.-W.; Chan, K.-H.; Cheng, V. C.-C.; Yuen, K.-Y. *J. Clin. Microbiol.* **2020**, *58*, No. e00936-20.

(20) Prince, H. E.; Givens, T. S.; Lapé-Nixon, M.; Clarke, N. J.; Schwab, D. A.; Batterman, H. J.; Jones, R. S.; Meyer, W. A.; Kapoor, H.; Rowland, C. M.; Haji-Sheikhi, F.; Marlowe, E. M. *J. Clin. Microbiol.* **2020**, *58*, No. e01742-20.

(21) Diao, B.; Wen, K.; Chen, J.; Liu, Y.; Yuan, Z.; Han, C.; Chen, J.; Pan, Y.; Chen, L.; Dan, Y.; Wang, J.; Chen, Y.; Deng, G.; Zhou, H.; Wu, Y. *medRxiv* **2020**, *2020*, 03.07.20032524.

(22) Huang, L.; Muyldermans, S.; Saerens, D. *Expert Rev. Mol. Diagn.* **2010**, *10*, 777−785.

(23) Salvador, J.-P.; Vilaplana, L.; Marco, M.-P. *Anal. Bioanal. Chem.* **2019**, *411*, 1703−1713.

(24) De Meyer, T.; Muyldermans, S.; Depicker, A. *Trends Biotechnol.* **2014**, *32*, 263−270.

(25) Hoey, R. J.; Eom, H.; Horn, J. R. *Exp. Biol. Med.* **2019**, *244*, 1568−1576.

(26) Esparza, T. J.; Martin, N. P.; Anderson, G. P.; Goldman, E. R.; Brody, D. L. *Sci. Rep.* **2020**, *10*, 22370.

(27) Hanke, L.; Vidakovics Perez, L.; Sheward, D. J.; Das, H.; Schulte, T.; Moliner-Morro, A.; Corcoran, M.; Achour, A.; Karlsson Hedestam, G. B.; Hällberg, B. M.; Murrell, B.; McInerney, G. M. *Nat. Commun.* **2020**, *11*, 4420.

(28) Xiang, Y.; Nambulli, S.; Xiao, Z.; Liu, H.; Sang, Z.; Duprex, W. P.; Schneidman-Duhovny, D.; Zhang, C.; Shi, Y. *Science* **2020**, *370*, 1479.

(29) Goldman, E. R.; Anderson, G. P.; Liu, J. L.; Delehanty, J. B.; Sherwood, L. J.; Osborn, L. E.; Cummins, L. B.; Hayhurst, A. *Anal. Chem.* **2006**, *78*, 8245−8255.

(30) Liu, J. L.; Shriver-Lake, L. C.; Anderson, G. P.; Zabetakis, D.; Goldman, E. R. *Microb. Cell Fact.* **2017**, *16*, 223.

(31) Liu, J.; Shriver-Lake, L. C.; Zabetakis, D.; Anderson, G. P.; Goldman, E. R. *Mol. Immunol.* **2019**, *105*, 190−197.

(32) Shriver-Lake, L. C.; Liu, J. L.; Zabetakis, D.; Sugiharto, V. A.; Lee, C.-R.; Defang, G. N.; Wu, S.-J. L.; Anderson, G. P.; Goldman, E. R. *Sci. Rep.* **2018**, *8*, 18086.

(33) Corpet, F. *Nucleic Acids Res.* **1988**, *16*, 10881−10890.

(34) Walper, S. A.; Liu, J. L.; Zabetakis, D.; Anderson, G. P.; Goldman, E. R. *PLoS One* **2014**, *9*, No. e106263.

(35) Liu, J. L.; Webb, E. M.; Zabetakis, D.; Burke, C. W.; Gardner, C. L.; Glass, P. J.; Legler, P. M.; Weger-Lucarelli, J.; Anderson, G. P.; Goldman, E. R. *Front. Med.* **2021**, *8*, 12.

(36) Hopkins, N. A. E. Protein expression. U.S. Patent 20110177615 A1, 2011.

(37) Shriver-Lake, L. C.; Zabetakis, D.; Goldman, E. R.; Anderson, G. P. *Toxicon* **2017**, *135*, 51−58.

(38) Glaven, R. H.; Anderson, G. P.; Zabetakis, D.; Liu, J. L.; Long, N. C.; Goldman, E. R. *Biosensors* **2012**, *2*, 43.

(39) Anderson, G. P.; Liu, J. L.; Shriver-Lake, L. C.; Zabetakis, D.; Sugiharto, V. A.; Chen, H.-W.; Lee, C.-R.; Defang, G. N.; Wu, S.-J. L.; Venkateswaran, N.; Goldman, E. R. *Anal. Chem.* **2019**, *91*, 9424−9429.

(40) Goldman, E. R.; Liu, J. L.; Zabetakis, D.; Anderson, G. P. *Front. Immunol.* **2017**, *8*, 865.

(41) Turner, K. B.; Liu, J. L.; Zabetakis, D.; Lee, A. B.; Anderson, G. P.; Goldman, E. R. *Biotechnol. Rep.* **2015**, *6*, 27−35.

(42) Chang, C.-k.; Sue, S.-C.; Yu, T.-h.; Hsieh, C.-M.; Tsai, C.-K.; Chiang, Y.-C.; Lee, S.-j.; Hsiao, H.-h.; Wu, W.-J.; Chang, C.-F.; Huang, T.-h. *FEBS Lett.* **2005**, *579*, 5663−5668.

(43) Hultberg, A.; Temperton, N. J.; Rosseels, V.; Koenders, M.; Gonzalez-Pajuelo, M.; Schepens, B.; Ibanez, L. I.; Vanlandschoot, P.; Schillemans, J.; Saunders, M.; Weiss, R. A.; Saelens, X.; Melero, J. A.; Verrips, C. T.; Van Gucht, S.; de Haard, H. J. *PLoS One* **2011**, *6*, No. e17665.

(44) Conrath, K. E.; Lauwereys, M.; Wyns, L.; Muyldermans, S. *J. Biol. Chem.* **2001**, *276*, 7346−7350.

(45) Anderson, G. P.; Taitt, C. R. *Sens. Lett.* **2008**, *6*, 213−218.

(46) Tilocca, B.; Soggiu, A.; Sanguinetti, M.; Musella, V.; Britti, D.; Bonizzi, L.; Urbani, A.; Roncada, P. *Microbes Infect.* **2020**, *22*, 188−194.

(47) Ye, Q.; West, A. M. V.; Silletti, S.; Corbett, K. D. *Protein Sci.* **2020**, *29*, 1890−1901.

(48) Wrapp, D.; De Vlieger, D.; Corbett, K. S.; Torres, G. M.; Wang, N.; Van Breedam, W.; Roose, K.; van Schie, L.; Hoffmann, M.; Pöhlmann, S.; Graham, B. S.; Callewaert, N.; Schepens, B.; Saelens, X.; McLellan, J. S. *Cell* **2020**, *181*, 1436−1441.

(49) Li, W.; Schäfer, A.; Kulkarni, S. S.; Liu, X.; Martinez, D. R.; Chen, C.; Sun, Z.; Leist, S. R.; Drelich, A.; Zhang, L.; Ura, M. L.; Berezuk, A.; Chittori, S.; Leopold, K.; Mannar, D.; Srivastava, S. S.; Zhu, X.; Peterson, E. C.; Tseng, C.-T.; Mellors, J. W.; Falzarano, D.; Subramaniam, S.; Baric, R. S.; Dimitrov, D. S. *Cell* **2020**, *183*, 429−441.

(50) Sherwood, L. J.; Hayhurst, A. *ACS Synth. Biol.* **2021**, *10*, 379−390.

(51) Raphael, M. P.; Christodoulides, J. A.; Byers, J. M.; Anderson, G. P.; Liu, J. L.; Turner, K. B.; Goldman, E. R.; Delehanty, J. B. *Plasmonics* **2015**, *10*, 1649−1655.